Journal of Civil Engineering Researchers

J-Researchers

JOURNAL OF CIVIL ENGINEERING RESEARCHERS

Three-dimensional simulation of granular materials by discrete element method (DEM) by considering the fracture effect of particles

Amir Mahboob[a], Omid Hassanshahi[b,c *], Ashkan Sarabi Tabrizi[d]

[a] *Department of Civil, Water and Environmental Engineering, Shahid Beheshti University, Tehran, Iran*

[b] *Department of Civil engineering, University of Minho, Campus de Azurém, 4800-058, Guimarães, Portugal*

[c] *Institute for Sustainability and Innovation in Structural Engineering, University of Minho, 4800-058, Guimarães, Portugal*

[d] *Department of Civil Engineering, Science and Culture University, Tehran, Iran*

Journals-Researchers use only: Received date: 2023.03.20; revised date: 2023.04.15; accepted date: 2023.04.20

Abstract

Coarse-grained materials, such as sand and gravel, exhibit a significant dependence on particle failure rate, which greatly influences their engineering behavior. This research focuses on the three-dimensional modeling of grain material behavior using the discrete element method (DEM) with PFC3D software and FISH programming language. The specific objective is to model the particle breakage phenomenon and its impact on resistance behavior and deformation. To accurately represent the non-spherical shape of the particles, an interconnected sphere approach was employed. The modeling of grain failure was achieved by establishing a failure criterion that considers two critical conditions: the heterogeneity of contact forces and stress within the particle. The proposed model and criteria were validated through comparison with triaxial experimental results obtained from the Purulia dam gravel. The results demonstrate that the developed model successfully captures the essential aspects of particle failure and its influence on the behavior of the granular environment. The simulations accurately represent the resistance behavior and deformation characteristics observed in the triaxial experiments. This validates the effectiveness of the proposed model in simulating the significant effects of particle failure on the behavior of coarse-grained materials. The findings of this study contribute to a deeper understanding of the complex behavior of coarse-grained materials, particularly in terms of their response to particle failure. The developed DEM model, incorporating the particle breakage phenomenon, provides a valuable tool for accurately predicting and analyzing the behavior of granular materials in various engineering applications. (DOI:**https//doi.org/10.52547/JCER.5.2.14**)

Keywords: discrete component method; fracture effect; three-dimensional simulation; granular materials.

* Corresponding author. Tel.: +0-351913837461; e-mail: omid.hasanshahi@civil.uminho.pt.

1. Introduction

Grain environments are composed of separate particles, these particles are independent of each other and affect each other only at the points of contact. The behavior of these materials is complex and several experiments are required to determine this behavior. The behavior of granular soils such as sand is affected by the applied stress on the complex. At high stresses, soil particles can become brittle. Fracture of particles and conversion of coarse particles into smaller particles causes changes in the granulation curve and as a result change in the technical properties of granular materials. This phenomenon occurs more in tall earthen structures such as gravel dams and breakwaters, especially in the lower layers, which under the weight of the upper layers experience greater stresses. With the development of rapid computing, numerical methods are becoming more widely used to model the behavior of aggregates [1, 2]. One of these methods, which is developing more and more today, is the separate components method [3, 4].

The discrete method is a numerical method developed by Kandal to analyze rock mechanics problems [5, 6]. This method was used in 1979 by Kandal and Strack to simulate the behavior of a set of granular particles [7]. By comparing the force obtained from the numerical method and the results of the experimental photovoltaic method, they showed that the discrete component method is a valid tool for basic studies of the behavior of grain assemblies. Research has shown that the discrete component method can simulate the actual and physical behavior of grain assemblies [4]. The discrete component (DEM) method uses simple contact rules at intergranular contact points to obtain complex set of material responses. This method tries to simulate its mechanical behavior without imposing a specific behavioral law on the material. It can also consider the effect of various factors (such as grain shape, grain size and grain strength, etc.) on the mechanical behavior of the soil under study. One of the most important phenomena whose effect on the behavior of grain materials has been proven by many researchers is the phenomenon of grain failure [8, 9, 10 and 11]. Fracture of grains reduces the volume of voids and as a result the shrinkage behavior of materials, reduces shear strength and also reduces the hydraulic conductivity of materials [10, 12].

The failure rate of particles is affected by various factors. Zhou et al. [11], by studying the three-dimensional behavior of micro and macro aggregates under different stress paths, concluded that the failure rate is strongly related to all-round stress, deflection stress and stress path. There are two ways to consider the separate nature of soils. The first method is to modify models based on continuous environment mechanics by introducing additional rules that reflect soil microstructural changes, such as texture 3 [12], or to improve existing structural rules based on micromechanical studies on soil [14]. The second method considers the soil directly as a set of separate materials and its macroscopic and microscopic responses are collected under load, numerically, analytically or experimentally. This method has been widely used by micromechanical researchers [15 to 22].

Lim and McDoll [23] presented a model for the behavior of ballast materials used under railways using the discrete component method and with PFC3D software under edometer pressure. Munjiza et al. [24] and Munjiza [25] proposed a hybrid finite element method for simulating grains with irregular shapes. We and colleagues [26, 27] used this method to simulate the fracture of gravel particles by simulating potential fracture surfaces with adhesive joint surface elements without thickness 6. One of the most important researches to model the particle fracture effect by the discrete method method is the simulation of the behavior of gravel materials and the particle fracture effect using a probabilistic fracture model. Using brittle two-dimensional clusters, Delvarsh et al. Simulated the behavior of gravel materials used in earthen dams, especially considering the effect of particle refraction on deformation, and the significant effect of particle fracture on dam deformation during dewatering as well as the potential impact. The conclusion of a hand-picked block layer upstream and downstream of the dam in improving the stability of the dam [28].

McDowell et al. investigated the fracture of three-dimensional sand grains using the discrete component method to investigate the effect of size on strength. They modeled an aggregate particle into a mass of interconnected spheres and randomly removed a

number of spheres to obtain the strength and joint distribution and cracks with the desired Weibull modulus. They concluded that in composite particles where the spheres are in a hexagonal arrangement, when zero to 25% of the spheres are removed from the mass, size has almost no effect on the strength of the composite particle [29]. Using PFC3D software, Cheng et al. simulated the fracture masses by the discrete method by considering the loading speed in the triaxial test along the path of different stresses [30].

In this work, the heterogeneity approach is subsequently validated using DEM simulations of a triaxial test of a particle sample. Averaged stresses and strains are calculated in the course of the simulations resulting in stress–strain curves. Thereby, the influence of some DEM parameters on the resulting stresses and strains are analyzed. Therefore, the elastic and plastic parameters are fitted to the stress–strain curves of the triaxial tests. The most significant contribution of this paper is that we developed a practical breakage modeling technique in the context of DEM, which has the potential to capture the complex physical behavior of breakable granular materials.

2. Model used for gravel materials

In order to simulate particle fracture in a model, we make the separate components of the particles that make up the particle set from composite particles [31]. A composite particle, called a cluster, consists of a number of connected spherical grains (spheres) that, after breaking the cluster, the spherical particles can be separated from the group of particles, thus simulating the breakdown and separation of particles. It becomes malleable in a composite particle. In the present simulation, three-dimensional composite particles made of spherical spheres of different sizes have been used to model the gravel grains and the possibility of modeling their fracture. We also use finer spheres attached to the clusters of the previous type to consider the angular shape of the gravel material after fracture. The connection of these tiny spheres to the larger spheres is such that the tiny spheres cannot be separated from their host spheres. The production of pebble blocks is such that first the items forming each pebble block (cluster) are produced together and the relative position of the items forming each pebble cluster remains constant during the simulation, unless the satisfaction failure criterion in this case, the spheres forming the cluster are separated from each other, and in this way, the simulation of particle failure is performed in this method. In order to simulate failure and create this capability in PFC3D software [32, 33], the necessary subroutines in the FISH programming language (FISH) were added to the main coding software and added to it. For every 100 cycles of simulation, these subroutines are called and executed. In this way, all the gravel clusters are controlled in the defined failure criterion, and the items or sub-clusters that make up each cluster that meet the failure criterion are separated according to the failure pattern, and then the simulation they will act freely and independently. In order to prevent the occurrence of large forces during the failure of particles, during the production of a cluster, the particles do not overlap and also at the moment of failure of the cluster, in a few steps or zero particle velocity to reduce kinetic energy and unbalance the spheres by coding Properly done.

2.1. Arrangement of clusters

In this study, two groups of clusters have been used to simulate gravel blocks. The clusters of the first group have no peripheral spheres and the clusters of the second group have tiny peripheral spheres. The first group of pebble clusters consisting of 4, 5, 6 and 8 spheres in three directions x, y and z are shown in Figures 1 to 4, respectively. In the first group, there are clusters of 4 spheres, 2 types of spheres with radii of 0.75 and 0.5 cm (Figure 1), which are surrounded by a hypothetical sphere with a diameter of 3 cm (similar to - Construction of gravel block with a diameter of 3 cm).

For clusters of 5 spheres (Figure 2), all the spheres that make up the cluster are the same (approximately 1.16 cm in radius). The cluster is enclosed in a hypothetical sphere 5 cm in diameter (simulation of a 5 cm diameter gravel block). Also, for clusters consisting of 6 spheres, there is a type of sphere with equal radius (approximately 0.828 cm). The cluster is enclosed in a hypothetical sphere 4 cm in diameter (simulation of a 4 cm diameter gravel block).

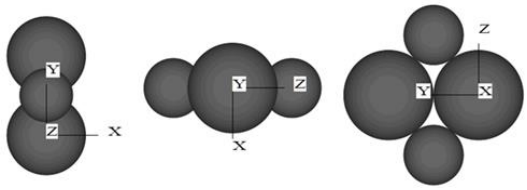

Figure 1: Cluster of the first group - the first type, consisting of 4 spheres.

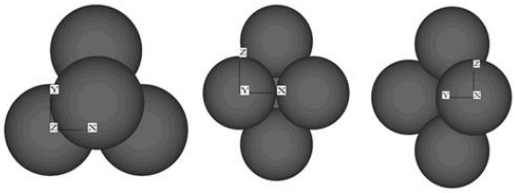

Figure 2: Cluster of the first group - the second type, consisting of 5 spheres.

Finally, for clusters of 8 spheres, there are two types of spheres. In order for the cluster to be enclosed inside a hypothetical sphere with a diameter of 6 cm (simulation of a pebble block with a diameter of 6 cm), the radii of the larger and smaller spheres are approximately equal to 1.39 and 0.9 cm, respectively. Also, for clusters consisting of 6 spheres, there is a type of sphere with equal radius (approximately 0.828 cm). The cluster is enclosed in a hypothetical sphere 4 cm in diameter (simulation of a 4 cm diameter gravel block).

Finally, for clusters of 8 spheres, there are two types of spheres. In order for a cluster to be enclosed within a hypothetical sphere 6 cm in diameter (simulation of a 6 cm diameter pebble block), the radii of the larger and smaller spheres are approximately equal to 1.39 and 0.39 cm, respectively.

The following clusters of the second group consisting of 4, 5, 6 and 8 spheres, in 3 directions x, y and z, are shown in Figures 5 to 8, respectively. As mentioned earlier, the clusters of the second group are similar to the clusters of the first group, except that they contain a number of tiny spheres whose radius is equal to one-eighth of the spheres attached to it in each cluster. There are two types of spheres, the corresponding sphere radius is considered (Figure 8).

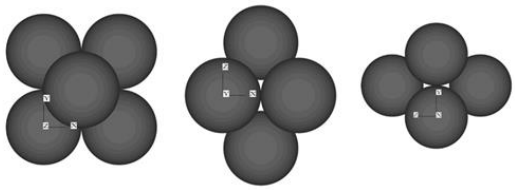

Figure 3: Cluster of the first group - the third type, consisting of 6 spheres.

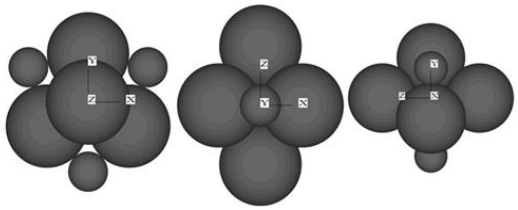

Figure 4: Cluster of the first group – the fourth type, consisting of 8 spheres.

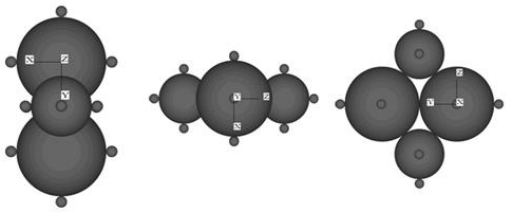

Figure 5: Cluster of the second group - the first type, consisting of 16 spheres.

A similar failure criterion has been used in previous studies [8, 34]. The blocks of the first group will be decomposed after breaking into their constituent spheres; The blocks of the second group, after failure, will be decomposed into their constituent clusters, which themselves contain several spheres. These sub-clusters can no longer be broken after the failure of the original cluster. The advantage of this type of cluster is that the particles left over from the fracture are angular, unlike the first group, where the particles from the fracture are completely round and spherical.

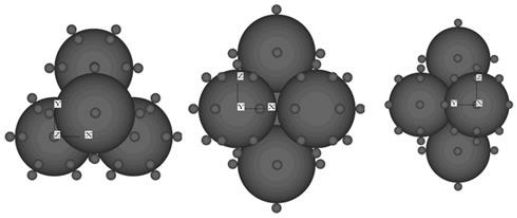

Figure 6: Cluster of the second group – the second type, consisting of 57 spheres.

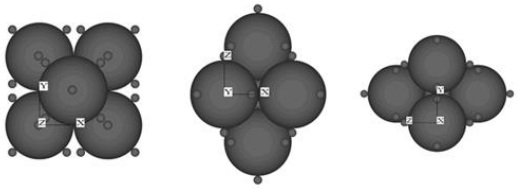

Figure 7: Cluster of the second group - the third type, consisting of 42 spheres.

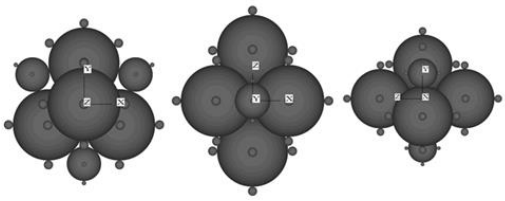

Figure 8: Cluster of the second group - the fourth type, consisting of 41 balls.

2.2. Failure criteria

In this study, in order to break a composite particle (cluster), it is necessary to fulfill two conditions simultaneously regarding the confinement of the cluster (inhomogeneity of the contact forces acting on a cluster) and the stress on the cluster:

The first condition: cluster confinement, in this research, the confinement failure condition related to confinement is measured using the contact force heterogeneity factor. If the coefficient of dissimilarity of the contact forces exceeds 0.25 (or in fact the confinement is less than a certain limit), one of the failure conditions is met.

The Second condition: the stress on the cluster is more than the defined failure resistance of each cluster.

2.3. Heterogeneity of contact forces for a cluster

For each cluster (pebble block), and for each angle θ, the ratio of the algebraic sum of all the contact forces in the θ direction to the total contact forces applied to that cluster is defined as the contact force orientation inequality. In order to enter the effect of contact force heterogeneity in the failure criterion, first condition is calculating the sum of contact forces for each cluster in the intervals Δφ, Δθ and Δψ (φ, θ and ψ are the angles of each point of contact in a cluster with three coordinate axes).

In this study, for the simplicity of the failure criterion and the computational volume, the forces will be calculated for the intervals Δθ=Δφ=Δψ =20°. This means that space is divided into three directions x, y and z in the range of 20 ° and each is assigned an identification number. For this purpose, all the space around each cluster is searched by writing three overlapping rings and examines all the contacts of a sphere forming a cluster and records the force applied based on the angle range inside it. This information is stored in a three-dimensional array that has 18 members in each dimension and is coded and added in the main software. This process is repeated for all contacts of other items in a cluster and then for all other clusters).

Then the largest element of this matrix is searched and it is represented by (fθ) max. The algebraic sum entered on a cluster is also calculated, which is denoted by ∑fθ. Finally, the heterogeneity factor of the spectator Uf, the correspondence of Equation (1) is calculated:

$$U_f = \frac{(f_\theta)_{max}}{\Sigma f_\theta} \qquad (1)$$

The value of Uf varies from zero to 0.5 (for point load testing).

2.4. Tension created in a cluster

To introduce the second condition of failure (related to failure resistance), it is first necessary to determine the stress created in the cluster due to contact forces. The maximum tensile stress created in the stone blocks under indirect tensile test is calculated according to the following equation [35]:

$$\sigma = \frac{F}{\bar{d}^2} \quad (2)$$

Where: F is the force exerted on the rock by the test plates and $\bar{d}$ is the distance between the test plates at the beginning of the test. Therefore, in the present model, assuming that the fracture mechanism of pebble blocks in a block set is similar to the fracture mechanism in the Brazilian experiment, the maximum tensile stress created in a cluster is calculated using the following equation:

$$\sigma_t = \frac{(f_\theta)_{max}}{\bar{d}^2} \quad (3)$$

(f_θ) max is calculated as mentioned before in section 2.3.

2.5. Fracture resistance

The fracture ability of gravel grains depends on the type of rock and its constituent minerals as well as the physical characteristics of the material such as size, shape and internal porosity of the grains. McDowell et al. [36] considered the concept of probability in the study of grain failure behavior. The probability of survival (non-breaking) of a grain (Psc) under σc stress applied in the failure test was defined as follows:

$$P_{sc} = (\sigma \geq \sigma c) / t_n \quad (4)$$

Where, σ is the maximum stress created in the rock block in the indirect tensile test and tn total number of test particles.

They also stated that Weibull distribution could model changes in the strength of granular materials. Studies have shown that the fracture toughness of granular materials follows Weibull's law [37]. In order to achieve a regular pattern for the distribution of strength of granular materials, they defined the probability of survival of a grain under tensile stress as a function of the ratio σ / σ0 (normalized stress) [36]:

$$P_S = \exp [- (\sigma/\sigma_0)^m] \quad (5)$$

In this regard, Ps is the probability of survival of a grain under tensile stress and σ0 is the characteristic stress under which 37% of (exp (-1)) grains remain unscathed. m is the Weibull modulus that determines how the probability of survival changes with changes in stress and decreases with increasing resistance.

Marsal presented a study on the fracture toughness of stone blocks as the mean Fb resistance (mean fracture toughness obtained from three experiments performed on a fixed type of material) [9]. He then proposed a relation for obtaining Fb from the diameter of the stone block:

$$F_b = \eta (d/d_0)^{\lambda} \quad (6)$$

In this regard, Fb is in terms of kilograms and η and λ are characteristic of the material and d0 is the characteristic size. Marcel first assumed that the parameter λ for pebbles was equal to 1.5. His additional studies showed that this assumption was not far from reality and for different pebble materials tested, the λ parameter was obtained between 1.2-1.8. Subsequent studies showed that there is a direct relationship between the Weibull modulus and the λ parameter [28]:

$$\lambda = 2-(3/m) \quad (7)$$

Therefore, by placing 1.5 instead of the parameter λ in the above equation, the value 6 is obtained for the Weibull modulus of the gravel material.

Thus, by obtaining m for these gravel materials, the probability-based resistance distribution can be obtained. In this study, for conducting experiments and simulations, the pebble characteristics provided by Varadarajan et al. [38]. In the results of their experiments, they did not mention the distribution based on the probability of gravel resistance and used the concept of failure value (percentage change through sieve) to investigate grain failure. Therefore, according to the studies performed on stone blocks by Marsal and according to the type of stone materials tested by Varadajan et al., The appropriate failure resistance for this problem is extracted. Table 1 shows the specifications of different materials tested by Varadarajan et al. [38]. Thus, by having the material properties of η and λ, we can obtain Fb and according

Table 1.
Specifications of stone materials tested by Varadarajan et al. [38].

Specimen	Type of materials	λ	η (N)	F_b (N)	d_{avg} (m)
Various stone materials tested by Marsal	Quartz	1/6	2218850	10900	0/04
	Diorite	1/2	351660	7030	0/042
	Basalt	1/4	883340	11400	0/043
	Granite	1/6	1315460	6030	0/04
Granular materials	Includes quartz, biotite and feldspar	1/5	1400000	11200	0/04

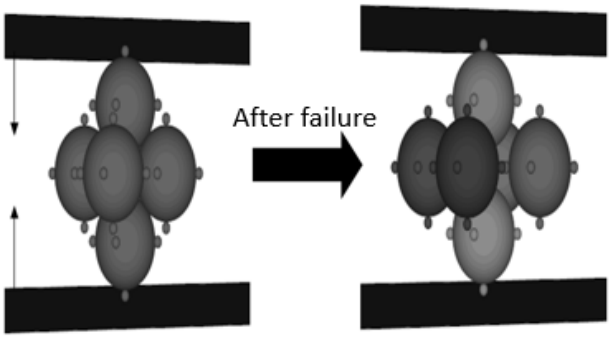

Figure 9. Indirect tensile test on the second group gravel block with 6 sub-clusters.

to equation (6), the resistance of the block with any diameter size.

In order to conform to the statistical distribution of Weibull with a modulus (m) equal to 6, the possible coefficients of resistance changes on the characteristic resistance (σ_0) have been applied. By extending Equation (5), the range of changes of the $\sigma/\sigma 0$ ratio from 0.0465 (for 99% survival probability) to 1.29 (for 1% survival probability) is obtained. Considering the fracture toughness (σ_{max}) equal to σ_0, the characteristic stress of the desired distribution ($\sigma 0$) will be equal to (σ_{max}) and the range of changes of the maximum tolerable stress of materials (σ_{max}) in the range ($0.465\sigma_0$-$1.29\sigma_0$) is obtained. PFC^{3D} software does not have the ability to generate such a distribution directly, so a suitable subroutine was added to the software.

3. Numerical failure tests on gravel blocks

In total, two types of indirect tensile numerical tests and triaxial tests have been simulated on samples made of different types of gravel blocks in different conditions. First, to extract the probability distribution of survival and validation of the failure model, the indirect tensile numerical test is simulated on the types of gravel blocks produced. In the following, various triaxial experiments have been performed and validated.

3.1. Fracture resistance

To extract the survival probability distribution of the modeled clusters, the clusters of the second group with 6 sub-clusters and 30 pebble blocks with the same diameter (4.4 cm) between two rigid walls, under

controlled strain conditions, were tested and experienced failure (Figure 9). The clusters produced in the second group are already shown in Figures (5) to (8). In this test, the walls approach each other at a uniform speed, and as mentioned in Section 2, the gravel block is checked once every 100 cycles for failure. If the failure criterion is true, the sub-clusters that make up the cluster will be separated. An example of a stress diagram applied to a cluster versus computational cycles is given in Figure 10. The declared stresses, using Equation (6) for the cluster are of unit thickness. The normal and tangential stiffnesses of the disks are equal to 1.5 x 10^8 N/m and the internal coefficient of friction is 0.7.

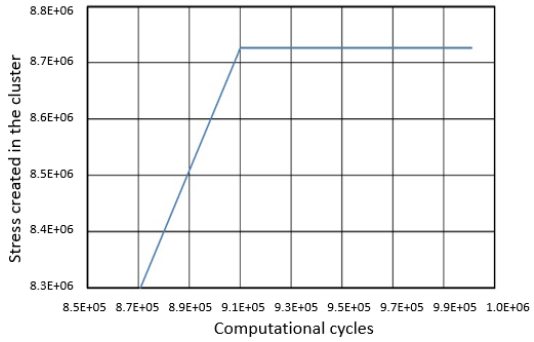

Figure 10: Stress created in the cluster (in Pa) against computational cycles.

Due to the scattering applied to the strength of the blocks, different maximum stresses were obtained from these experiments. Figure 11 shows the probability survival curve for Weibull distribution as well as the results of uniaxial experiments. In this form, the agreement between the numerical results and the Weibull distribution is clear.

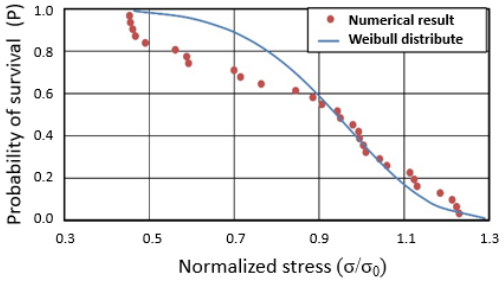

Figure 11. Probability of survival curve against normalized stress σ/σ_0.

After the experiments, a value of 8.389 MPa was obtained for σ0, which, as mentioned, can be considered as the fracture toughness of the material. Therefore, the fracture toughness of materials with a diameter of 4.4 cm is 389.8 MPa. This value is obtained according to the simulation performed; In the real case, considering the relations (2) and (6) and holding the diameter of the block, the real resistance can be obtained. This value is 6.67 MPa for a block with a diameter of 0.044 m, which indicates a good agreement between the actual results and the simulation. Equation (5) can be rewritten as follows, and used to determine the Weibull modulus.

$$\ln(\ln(1/P_S)) = m \times Ln(\sigma/\sigma_0) \quad (8)$$

4. Triaxial tests

In the present study, in order to validate the model, triaxial experiments performed by Varadarajan et al. On the pebble materials of Prolia Dam have been considered [37].

In Figure 12, both the Weibull distribution results and the numerical results give approximately the same value of m. In this figure, the slope of the curve, according to Equation 7 and the coordinate axes, is m.

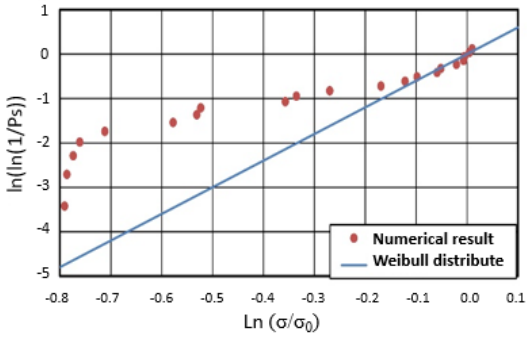

Figure 12. Modulus m, for Weibull distribution and performed tests.

4.1. How to perform triaxial experiments on the sample of gravel blocks

To simulate the triaxial experiment, a set of pebble blocks within six walls are considered as boundary

Table 2.
Sample characteristics in triaxial numerical simulations

Composition of clusters	Group type	Cluster diameter (cm)	Number of modeled spheres	Number of modeled clusters	Vertical and shear stiffness (N/m)	Density	Coefficient of wall friction with particles	Coefficient of friction between particles	Vacuum sign
First group	First	3	10900	2100	1×10^8	2680	0/7	0/25	0/66
	Second	5							
	Third	4							
	Fourth	6							
Second group	First	3.27	31316	1100	1×10^8	2680	0/7	0/25	0/7
	Second	5.58							
	Third	4.4							
	Fourth	6.7							

elements to apply boundary conditions. Horizontal walls are used as rigid plates to introduce vertical force and vertical walls are used to apply all-round stress. The normal and tangential stiffnesses of horizontal walls are equal to the stiffness of the clusters, but the stiffness of the vertical walls relative to 0.1 stiffness of the clusters is considered to simulate the conditions of soft confinement [30]. Dumping was equal to 0.7 (software default) and time step was 2E-6.

To prepare the test sample, a precipitation process was used to prevent distortion of the initial conditions of the sample. In general, triaxial experiments consist of three stages:

1. The first stage of making a sample with the desired porosity (which includes the process of falling clusters and moving the walls together).

2. The second stage of applying all-inclusive tension to the desired tension.

3. The third stage is the application of deviant stress with constant all-round stress.

It should be noted that in the first stage (sample making) the clusters are not allowed to fail, but in the second and third stages this is possible and the clusters are examined during the process specified in the failure criterion.

In the deflection stress application stage for cutting, the upper and lower horizontal walls of the specimen approach each other at a predetermined speed. This speed is low in the early stages and then increases in the later stages to reach the final speed (0.04 m/s).

The number of these steps is 80; in the first stage, the speed of the walls is 1.80, the final speed, at the end of the stage it reaches our final speed. Table 2 shows the specifications of the simulations.

4.2. Sample preparation steps

First, six walls were built at regular intervals to form a rectangular cube with dimensions of 2.6*1.1*1.1 meters, as shown in Figure 13. In this space, 2100 spheres with a varying radius of 3 to 6 cm are created at random, followed by 200 octagonal clusters (containing eight spheres), 500 5clusters, 600 6clusters, and 800 4clusters. Some of the original pieces are replaced (Figure 13-a). Then, by applying gravity to the bottom of the sample (negative acceleration) and by applying several cycles, the particles are precipitated. In this way, the sample is prepared for compaction to the desired porosity (Figure 13-b). Finally, we bring the walls closer together at a suitable speed to achieve the desired minimum porosity ratio (shown in Table 2) (Figure 13-c). For the clusters of the second group, we repeat exactly the same procedure to make a sample of particles with more angularity.

The final dimensions of the sample are 0.28*0.48*0.28 that the ratio of the smallest dimension of the sample to the size of the largest aggregate for the sample of the first and second groups is 4.76 and 4.17, respectively.

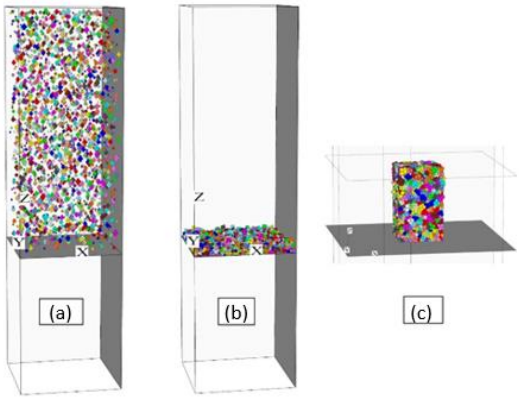

Figure 13. Sample preparation steps. a) Production of clusters b) Sedimentation of clusters, c) Movement of walls and compaction.

4.3. Applying all-round tension and deviant tension

Three-axis experiments are performed at various all-round pressures. To keep the overall stresses constant during the test, a lateral stress control mechanism was added to the software by coding. In this way, first the walls are approached to reach the desired stress, then by considering a small tolerance (for example, ±0.005 Pascal) the existing stress is compared with the all-round stress of the target and based on that the speed of the side walls is adjusted. Turns.

In PFC^{3D} software, we use movement and acceleration to the walls to load the sample (apply stress). In the deflection stress stage, the upper and lower walls of the specimen approach each other at a predetermined speed. This speed is low in the early stages and then increases in the later stages to reach the final speed (0.04 m/s). The number of these steps is 80; in the first stage, the speed of the walls is 1.80, and at the end of the stage, it reaches the final speed.

As mentioned, from the beginning of the all-inclusive stress phase to the end of the triaxial test, the clusters have the possibility of failure, although in the all-inclusive stress phase, only a small percentage of the clusters fail.

4.4. Triaxial tests' results

The results of triaxial experiments for the two groups of clusters and for all-round pressures of 0.3, 0.7 and 1 MPa are given, and finally the results of the two are compared. Figure 14 shows the failure rates of the clusters during the triaxial cutting section for all experiments.

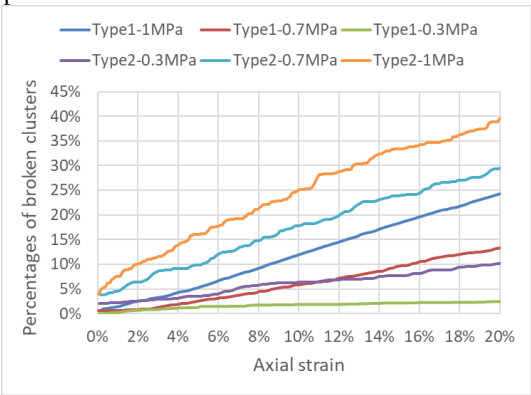

Figure 14. Percentages of broken clusters against axial strain (Clusters of the first and second groups, lateral stresses of 0.3 to 1 MPa).

The results show that the angularity of most of the simulated gravel blocks increases the failure slope of the clusters and its final percentage in strain by 20%, so that this trend for the second group cluster with all-round stress of 0.3 MPa is relatively similar to the first group cluster but with all-round stress is 0.7 MPa. For higher stresses (0.7 and 1 MPa) this difference is greater and the failure of the second group of clusters (sharp angle) is steeper. Table 3 shows the failure rate of clusters at 20% strain.

Table 3.

Percentage of cluster failure at 20% strain

Failure rate of clusters (%)

First group	Second group	All-round stress (kPa)	Failure rate (%)
4.64	18.10	300	119.4
14.29	30	700	109.9
25.57	40.18	1000	57.1

4.4.1 Comparison of stress and strain diagrams for each cluster group

Figures 15 to 18 show the diagrams of the deflection stress versus strain and volumetric behavior of the specimens during the triaxial test in all three all-round stresses for both groups of clusters, respectively.

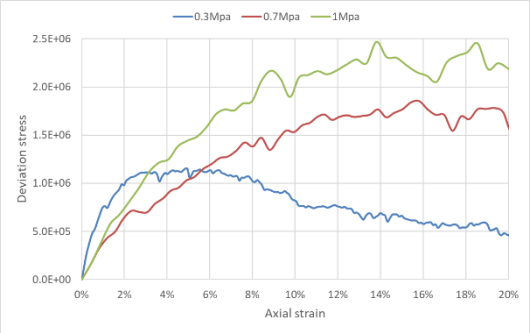

Figure 15. Deviation stress versus axial strain (first group cluster, all-inclusive stress of 0.3, 0.7 and 1 MPa).

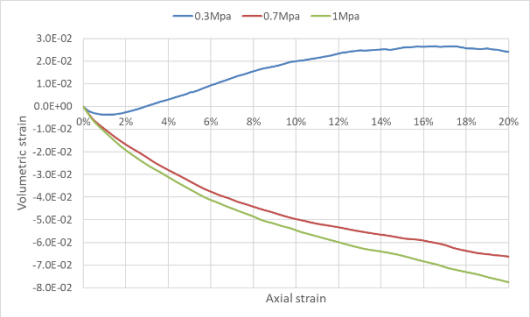

Figure 16. Volumetric strain of the first group cluster in all-round stress of 0.3, 0.7 and 1 MPa.

As mentioned earlier, for the clusters of the first group, in the all-round stress of 0.3 MPa, the sample behavior is different and has a peak, has a higher initial stiffness, but the amount of deflection stress in the strain is 20% less. There is also a difference between volumetric and axial strain behavior. According to Figure (16), only the sample under 0.3 all-inclusive stress showed diphtheria behavior, while the behavior of 0.7 and 1 MPa all-inclusive stress samples is completely contractile and decreases in volume.

The behavior is different for the clusters of the second group as shown in Figure (17). The sample from the all-inclusive stress of 0.3 MPa to 0.7 MPa experienced more deviation stress at constant strain, while the behavior of the samples with the all-inclusive stress of 0.7 and 1 MPa did not differ as much. In addition, as shown in Figure (18), the greater the overall stress, the higher the contractile behavior of the specimens.

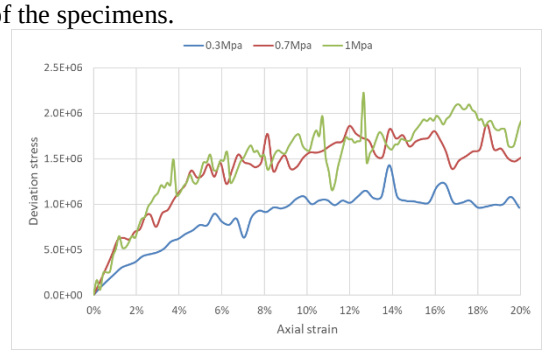

Figure 17. Deviation stress versus axial strain (second group cluster in all-round stress of 0.3, 0.7 and 1 MPa).

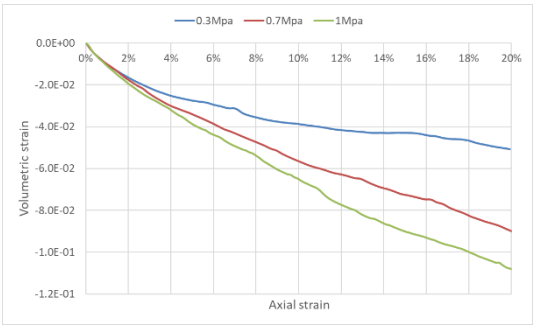

Figure 18. Volumetric strain versus axial strain (second group cluster in all-round stress of 0.3, 0.7 and 1 MPa).

4.4.2 Comparison of stress and strain diagrams for each all-round stress

In this section, the behavior of the samples at different all-round stresses for the two groups of clusters is presented separately to determine more precisely the effect of roundness or sharpness of the gravel blocks. In the 0.3 MPa all-round stress, the round specimen (first group) has a peak, while the sharp specimen (second group) has a fixed concavity direction with a certain amount of stress (Figure 19).

Also, the round specimen (first group) has a contractile and dilated behavior, while the sharp specimen (second group) is completely contractile (Figure 20), which is a function of the greater failure

of the second group of gravel particles. Fracture of the pebble and production of smaller particles causes more contractile behavior.

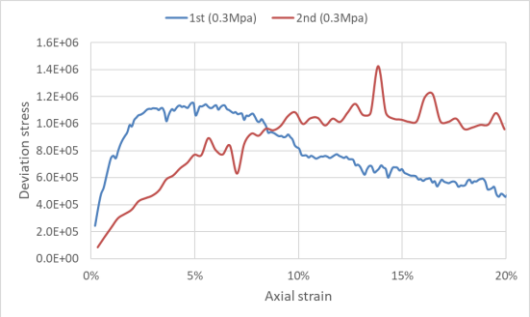

Figure 19. Deviation stress versus axial strain (first and second group clusters, all-round stress 0.3 MPa).

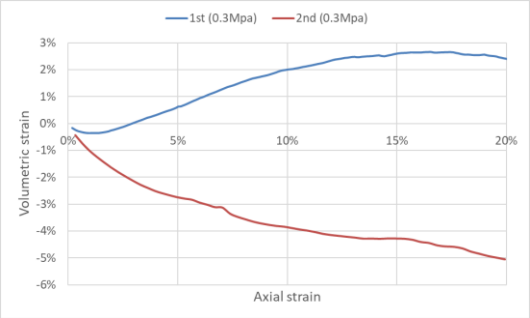

Figure 20. Axial strain versus volumetric strain (first and second group clusters, all-round stress 0.3 MPa).

At an all-round stress of 0.7 MPa, the sharp-edged specimen (second group), compared to the first group, initially establishes greater amounts of stress per strain and then almost coincides and behaves in a similar manner (see Figure 21).

Also, both round (first group) and sharp (second group) specimens have contractile behavior, which is more for the sharp corner (second group), see Figure 22.

In the 1MP all-round stress, first the diagrams of the two samples are almost identical and then the round sample (first group) shows higher values of stress per strain (Figure 23). Also, as in the experiment with all-round stress of 0.7 MPa, both specimens of round (first group) and sharp (second group) have contractile behavior, which is higher for sharp specimens (Figure 24).

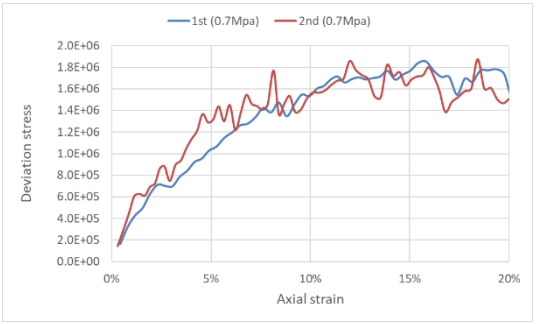

Figure 21. Deviation stress versus axial strain (first and second group clusters, all-round stress 0.7 MPa).

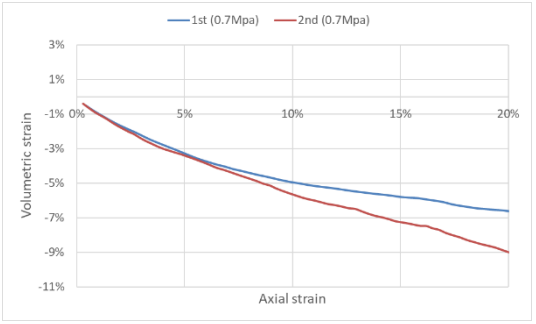

Figure 22. Axial strain versus volumetric strain (first and second group clusters, all-round stress equal to 0.7 MPa).

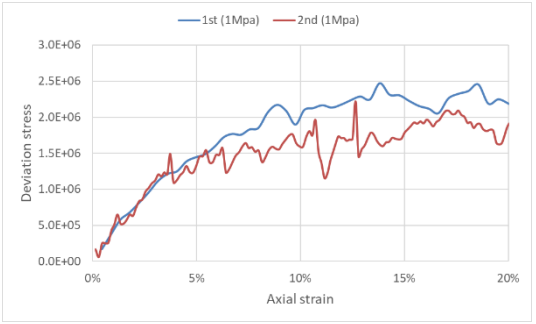

Figure 23. Deviation stress versus axial strain (clusters of the first and second groups, all-inclusive stress of 1 MPa).

4.5. Granulation change due to particle failure

The granulation curves for the samples at the end of the isotropic density and the end of the experiment are shown in Figure 25. It can be seen that with increasing lateral stress, the failure in the sample increases and the changes in the grain size curve

increase. Also, with increasing particle angulation (cluster of the second group), the failure has increased and the grain size of the sample has become finer.

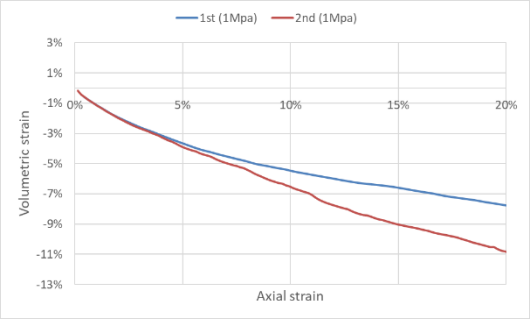

Figure 24. Axial strain versus volumetric strain (clusters of the first and second groups, all-inclusive stress of 1 MPa).

4.5. Granulation change due to particle failure

The granulation curves for the samples at the end of the isotropic density and the end of the experiment are shown in Figure 25. It can be seen that with increasing lateral stress, the failure in the sample increases and the changes in the grain size curve increase. Also, with increasing particle angulation (cluster of the second group), the failure has increased and the grain size of the sample has become finer.

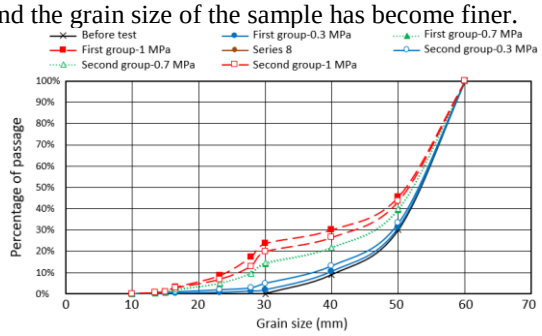

Figure 25. Grading curves of materials before and after testing.

4.6. Comparison of simulation results with experimental results

The results of the experiments performed in Section (4.4) together with the data obtained from large-scale triaxial experimental experiments on dam materials (Sample B) [38] in Figures 26 and 27 and also in Table 4 are given.

Figure 26 Comparison of stress and axial strain results of simulated experiments (for the first group cluster) and reported results for experimental experiments [38] with all-round stresses of 0.3 and 0.9 MPa and also Figure 27 Volumetric strain results against axial strain for the same experiments.

In order to save time and number of simulations, three all-round pressures of 0.3, 0.7 and 1 MPa have been used for the simulations. The experimental experiments were performed in four all-round stresses of 0.3, 0.6, 0.9 and 1.2 MPa. The simulated experiments are in the middle of the experimental experiments. Due to the limitations of simulation, the initial porosity of the samples is different, so the volumetric strain of the simulated results and experimental experiments are not comparable. It should be noted that it was not possible to achieve low porosity in the three-dimensional preparation of the sample.

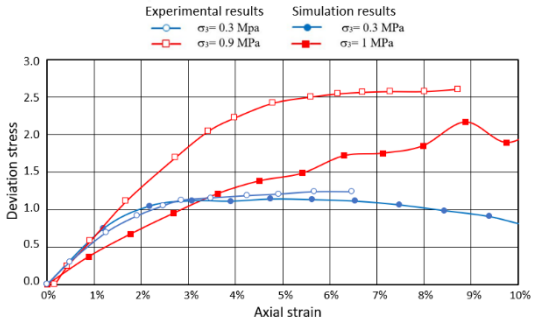

Figure 26. Comparison of axial strain versus deviation stress results for simulated samples and experimental results [38].

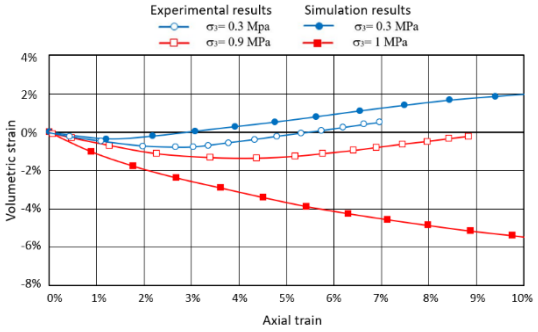

Figure 27: Comparison of axial strain versus volumetric strain results for simulated samples and experimental results [38].

Examination and comparison of the results show that the results in all-round stress of 0.3 MPa are quite

satisfactory, but with increasing all-round stress and increasing particle breakage in the numerical sample and due to the production of completely spherical particles resulting from composite particle failure, the numerical sample increases. It shows less resistance and has a more compact behavior in terms of volume.

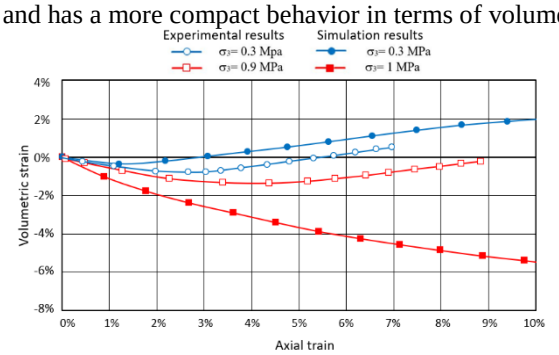

Figure 27: Comparison of axial strain versus volumetric strain results for simulated samples and experimental results [38].

Table 4.
Comparison of experimental and numerical results.

Simulation results			
First group clusters	Second group clusters	Experimental results	All-round stress
φ° in rupture		*φ° in rupture*	
41	40	43	0.3
35	33	38	0.7
28	34	36	1

Comparison of the values in Table (4) shows the high accuracy and consistency of the numerical simulation and the criteria presented with the experimental experiments. The decrease in φ for the second group clusters is greater than the first group due to the failure that occurred in the sample.

5. Conclusions

In this research, the behavior of gravel materials and the phenomenon of particle fracture have been simulated and validated using a discrete component method and an efficient model. As is clear from the output of the numerical tests:

1. Increasing the all-round pressure and increasing the sharpness of the gravel blocks has increased the grain failure during cutting to the sample. Particle breakage causes the specimens to show mostly no dilatation behavior and to act completely contractile.

2. The stress-strain behavior changes from dense (with peak) to the process of a loose sample, which all proves the high impact of the failure phenomenon on the sample behavior. The present study demonstrates the ability of the discrete component (DEM) method to consider the complex behavior of gravel materials.

3. The results obtained for simulating a real gravel show that the internal friction angle of the materials is simulated with good accuracy.

4. The following are the important characteristics and strengths of this model to simulate the behavior of gravel materials:

a) The proposed rupture criterion takes into account the resistance parameters as well as the confinement (heterogeneity of contact forces).

b) The concept of probability for the strength of blocks is included in the rupture criterion.

c) The three-dimensional model makes the results more accurate and the model more efficient.

References

[1] Salles, A., Salati, M. and Bragança, L., 2023. Analyzing the Feasibility of Integrating Urban Sustainability Assessment Indicators with City Information Modelling (CIM). Applied System Innovation, 6(2), p.45.

[2] Abedi, M., Hassanshahi, O., Rashiddel, A., Ashtari, H., Meddah, M.S., Dias, D., Arjomand, M.A. and Choong, K.K., 2023. A sustainable cementitious composite reinforced with natural fibers: An experimental and numerical study. Construction and Building Materials, 378, p.131093.

[3] Oh, C.L., Choong, K.K., Nishimura, T., Kim, J.Y. and Hassanshahi, O., 2019. Shape change analysis of tensegrity models. Latin American Journal of Solids and Structures, 16.

[4] O'Sullivan, C. (2011). Particle-based discrete element modeling: geomechanics perspective. International Journal of Geomechanics, 11(6), 449-464.

[5] Cundall, P. A. (1971). A computer model for simulating progressive large scale movements in blocky system. In Proc. Int. Symp. on Rock Fractures. (pp. II-8).

[6] Candall, P. A. (1974). A Computer model for rock-mass behavior using interactive graphics for the imput and output of geometrical data. Report MDR-2-74.

[7] Cundall, P. A., & Strack, O. D. (1979). A discrete numerical model for granular assemblies. geotechnique, 29(1), 47-65.

[8] Mahboob, A., Hassanshahi, O., Hakimi, A., & Safi, M. (2023). Evaluating the Performance of Hollow Core Slabs (HCS)-Concrete and Simplifying Their Implementation. Recent Progress in Materials, 5(2), 1-15.

[9] AtashBahar, M., Chenari, R. J., & e Neshaei, M. A. L. Evaluation of the Behavior of Rockfill Material Using Large-Scale Triaxial Tests.
[10] Salati, M., Bragança, L. and Mateus, R., 2022. Sustainability Assessment on an Urban Scale: Context, Challenges, and Most Relevant Indicators. Applied System Innovation, 5(2), p.41.
[11] Lade, P. V., Yamamuro, J. A., & Bopp, P. A. (1996). Significance of particle crushing in granular materials. Journal of Geotechnical Engineering, 122(4), 309-316.
[12] Yousefi, A., Bunnori, N.M., Khavarian, M., Hassanshahi, O. and Majid, T.A., 2017, October. Experimental investigation on effect of multi-walled carbon nanotubes concentration on flexural properties and microstructure of cement mortar composite. In AIP Conference Proceedings (Vol. 1892, No. 1, p. 020032). AIP Publishing LLC.
[13] Xu, M., Hong, J., & Song, E. (2017). DEM study on the effect of particle breakage on the macro-and micro-behavior of rockfill sheared along different stress paths. Computers and Geotechnics, 89, 113-127.
[14] Wan, R. G., & Guo, P. J. (2004). Stress dilatancy and fabric dependencies on sand behavior. Journal of Engineering Mechanics, 130(6), 635-645.
[15] Zhujiang, S. (1999). A granular medium model for liquefaction analysis of sands. CHINESE JOURNAL OF GEOTECHNICAL ENGINEERING-CHINESE EDITION-, 21(6), 742-748.
[16] Abedi, M., Hassanshahi, O., Barros, J.A., Correia, A.G. and Fangueiro, R., 2022. Three-dimensional braided composites as innovative smart structural reinforcements. Composite Structures, 297, p.115912.
[17] Chang, C. S., & Liao, C. L. (1990). Constitutive relation for a particulate medium with the effect of particle rotation. International Journal of Solids and Structures, 26(4), 437-453.
[18] Chang, C. S., & Ma, L. (1991). A micromechanical-based micropolar theory for deformation of granular solids. International Journal of Solids and Structures, 28(1), 67-86.
[19] Hassanshahi, O., Majid, T.A., Lau, T.L., Yousefi, A. and Tahara, R.M.K., 2017, October. Seismic performance of the typical RC beam–column joint subjected to repeated earthquakes. In AIP Conference Proceedings (Vol. 1892, No. 1, p. 120014). AIP Publishing LLC.
[20] Oda, M., Konishi, J., & Nemat-Nasser, S. (1982). Experimental micromechanical evaluation of strength of granular materials: effects of particle rolling. Mechanics of materials, 1(4), 269-283.
[21] Chang, C. S., & Liao, C. L. (1990). Constitutive relation for a particulate medium with the effect of particle rotation. International Journal of Solids and Structures, 26(4), 437-453.
[22] Chang, C. S., & Ma, L. (1991). A micromechanical-based micropolar theory for deformation of granular solids. International Journal of Solids and Structures, 28(1), 67-86.
[23] Lim, W. L., & McDowell, G. R. (2005). Discrete element modelling of railway ballast. Granular Matter, 7, 19-29.
[24] Munjiza, A., Owen, D. R. J., & Bicanic, N. (1995). A combined finite-discrete element method in transient dynamics of fracturing solids. Engineering computations.
[25] Munjiza, A. A. (2004). The combined finite-discrete element method. John Wiley & Sons.
[26] Ma, G., Zhou, W., & Chang, X. L. (2014). Modeling the particle breakage of rockfill materials with the cohesive crack model. Computers and Geotechnics, 61, 132-143.
[27] Ma, G., Zhou, W., Chang, X. L., & Chen, M. X. (2016). A hybrid approach for modeling of breakable granular materials using combined finite-discrete element method. Granular Matter, 18, 1-17.
[28] Deluzarche, R., & Cambou, B. (2006). Discrete numerical modelling of rockfill dams. International journal for numerical and analytical methods in geomechanics, 30(11), 1075-1096.
[29] McDowell, G. R., & Harireche, O. (2002). Discrete element modelling of soil particle fracture. Géotechnique, 52(2), 131-135.
[30] Cheng, Y. P., Nakata, Y., & Bolton, M. D. (2003). Discrete element simulation of crushable soil. Geotechnique, 53(7), 633-641.
[31] Mahboob, A., Eskenati, A. R., & Moradalizadeh, S. (2021). Numerical Investigation and Cost Analysis of FRP-Concrete Unidirectional Hybrid Slabs. International Journal of Applied Mechanics and Engineering, 26(4), 156-166.
[32] Itasca, C. G. I. (2005). PFC3D (Particle Flow Code in Three Dimensions). Minneapolis, Minnesota, USA.
[33] Peen, W.Y., Keong, C.K. and Hassanshahi, O., 2019. Behaviour of hollow circular section with multiple perforations under compression, flexure and torsion. Latin American Journal of Solids and Structures, 16.
[34] Abedi, M., Sanivada, U.K., Mirian, S.A., Hassanshahi, O., Al-Jabri, K., Correia, A.G., Lourenço, P.B. and Fangueiro, R., 2023. A self-sensing and self-heating planar braided composite for smart civil infrastructures reinforcement. Construction and Building Materials, 387, p.131617.
[35] Jaeger, J. C. (1967, April). Failure of rocks under tensile conditions. In International Journal of Rock Mechanics and Mining Sciences & Geomechanics Abstracts (Vol. 4, No. 2, pp. 219-227). Pergamon.
[36] McDowell, G. R., Bolton, M. D., & Robertson, D. (1996). The fractal crushing of granular materials. Journal of the Mechanics and Physics of Solids, 44(12), 2079-2101.
[37] Weibull, W. (1951). A statistical distribution function of wide applicability. Journal of applied mechanics.
[38] Varadarajan, A., Sharma, K. G., Venkatachalam, K., & Gupta, A. K. (2003). Testing and modeling two rockfill materials. Journal of geotechnical and geoenvironmental engineering, 129(3), 206-218.
[39] P. Audebert, P. Hapiot, J. Electroanal. Chem. 361 (1993) 177.
[40] J. Newman, Electrochemical Systems, 2nd ed., Prentice-Hall, Englewood Cliffs, NJ, 1991.
[41] A.R. Hillman, in: R.G. Linford (Ed.), Electrochemical Science and Technology of Polymers, vol. 1, Journals-Researchers, IRAN, 1987, Ch. 5.
[42] B. Miller, Proc. 6th Australian Electrochem. Conf., Geelong, Vic., 19-24 Feb., 1984; J. Electroanal. Chem., 168 (1984) 91.
[43] Jones, personal communication, 1992.